Photodynamic therapy at ultra-low NIR laser power and X-Ray imaging using Cu_3BiS_3 nanocrystals

Srivani Veeranarayanan[1*], M. Sheikh Mohamed[1,2*], Aby Cheruvathoor Poulose[1*], Masuko Rinya[3], Yasushi Sakamoto[4], Toru Maekawa[1,2], D. Sakthi Kumar[1,2]#

[1]*Bio-Nano Electronics Research Centre, Toyo University, Kawagoe, 350-8585, Japan*

[2]*Graduate School of Interdisciplinary New Science, Toyo University, Kawagoe, 350-8585, Japan*

[3]*JEOL Ltd. Otemachi Nomura Bldg.13F, 2-1-1, Otemachi, Chiyoda, Tokyo, 100-0004, Japan*

[4]*Biomedical Research Centre, Division of Analytical Science, Saitama Medical University, Saitama 350-0495, Japan*

Supporting Information

*** Equal contributing Authors**

 # Corresponding author

Prof. D. Sakthi Kumar,

Ph: 81-492-39-1636

Fax: 81-492-34-2502

E-mail: sakthi@toyo.jp

Tables

Table S1. Brief literature overview of NIR mediated PDT therapy with nanoparticles (without any photosensitizers). As evident most of the reports utilized high concentration of the NPs and laser dose, leading to generation of heat during NIR therapy (the observed cell death arises due to temperature rise, rather than ROS generation). In the present work, we have utilized least concentration of NCs and therapy was conducted with minimal laser dose. No temperature rise was noted and the pertaining cell death is solely attributed to photodynamic therapeutic module.

Nanoparticle	**Wavelength**	**Concentration/ Mode of Injection**	**Laser Irradiance**	**Irradiation Time (sec)**	**Temperature Rise (◦C)**	**Ref**
Au Nanoshells	808 nm and 980 nm	6 mg/kg Intratumoral	150 mW/cm^2	600 - 780	6 - 10	1
Cu_2S	808 nm	15 mg/kg Intratumoral	600 mW/cm^2	100	15	2
$W_{18}O_{49}$ Nanowires	808 nm and 980 nm	15 mg/kg Intratumoral	200 mW/cm^2	540 – 660	10	3
$Cu_2(OH)PO_4$	1064 nm	4 mg/kg Intratumoral	2 W/cm^2	300 - 600	10 - 12	4
Au Nanoechinus	808, 915 and 1064 nm	40 mg/kg Intratumoral	130 mW/cm^2	600	4	5
Cs_xWO_3 Nanorods	880 and 1064 nm	40 mg/kg Intratumoral	2 W/cm^2	300 - 600	10	6
CuS	808 nm	24 mg/kg Intratumoral	1 W/cm^2	600	11	7
UCNP-GQD	980 nm	-	0.5 W/cm^2	1200	-	8
UCNP-$SnWO_4$ nanohybrids	980 nm	8 mg/kg Intratumoral	1.5 W/cm^2	900	-	9
Cu_3BiS_3 NCs	808 nm	2 mg/kg Intratumoral	10 mW/cm^2	900	0	**Present work**

Table S2. Behavioral details: the normal activities such as [Moving in the Cage: A; Eating: B, Drinking Water: C, Grooming: D, Alertness: E; Level of activity: Scale 1 (Least) to 5 (High)] of mice pre-and post treatment were analyzed.

Treatment	Day 0	Day 15
Control	$A^5B^5C^5D^5E^5$	$A^2B^1C^3D^4E^5$
Control + NIR	$A^5B^5C^5D^5E^5$	$A^2B^1C^2D^5E^5$
Cu_3BiS_3	$A^5B^5C^5D^5E^5$	$A^1B^2C^3D^5E^5$
Cu_3BiS_3 + NIR	$A^5B^5C^5D^5E^5$	$A^5B^5C^5D^5E^5$

Table S3. The blood biochemical parameters of Cu_3BiS_3 administered mice remained comparable with control. The indicative numerical values are the results obtained by quantitative biochemical analysis.

Analyte	Control	Cu_3BiS_3 (24 h)	Cu_3BiS_3 (2 Wk)	Unit
TP	5 ± 1	6.3 ± 2	6.1 ± 1.2	g/dL
ALB	2.3 ± 0.28	3.2 ± 0.37	3 ± 0.42	g/dL
A/G	0.9	1	1	A/G
BUN	17.4 ± 2.8	25.9 ± 0.8	18.8 ± 0.56	mg/dL
CRE	0.12 ± 2.4	0.14 ± 1.5	0.11 ± 0.25	mg/dL
UA	7.7 ± 0.9	3.2 ± 0.72	3.5 ± 0.23	mg/dL
AST	47 ± 10.8	74 ± 23	66 ± 18.7	IU/L
ALT	26 ± 2	27 ± 2.5	35 ± 3.2	IU/L
ALP	212 ± 12.8	185 ± 17.8	187 ± 16.9	IU/L
LDH	571 ± 62	748 ± 45	582 ± 67	IU/L
CK	99 ± 13.9	120 ± 17.9	90 ± 18.9	IU/L
LIP	37 ± 5	26 ± 6	34 ± 8.1	mg/dL
T-CHO	126 ± 11.9	100 ± 9.0	88 ± 12.2	mg/dL
GLU	193 ± 12	161 ± 16	165 ± 10.2	mg/dL

Figures

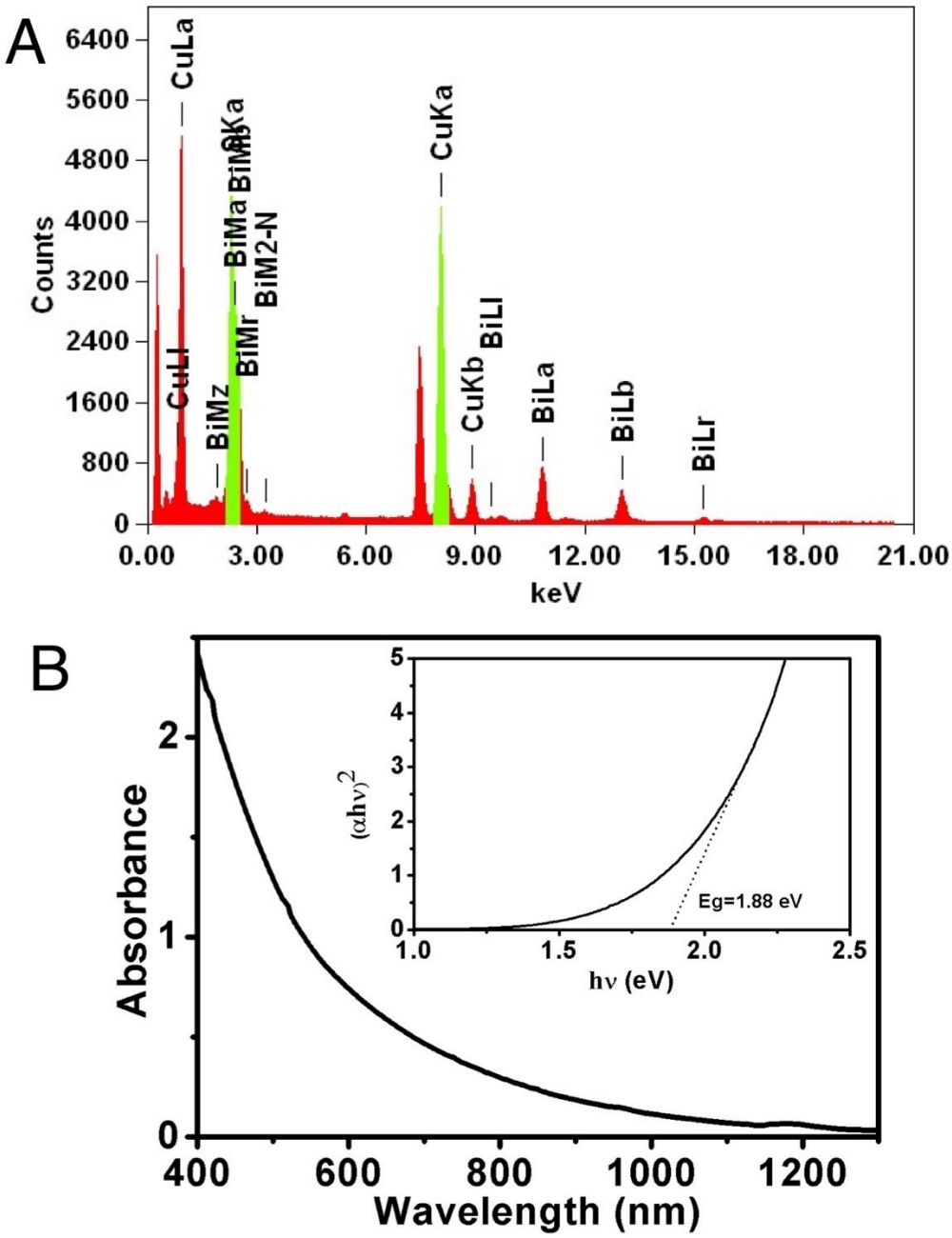

Figure S1. **(A)** EDS mapping of the as-synthesized NCs exhibiting the presence of Cu, Bi and S without other impurities. **(B)** Absorption spectra of as-synthesized NCs shows a broad absorption range spanning the NIR region. Bandgap of the NCs was calculated to be 1.88 eV (inset).

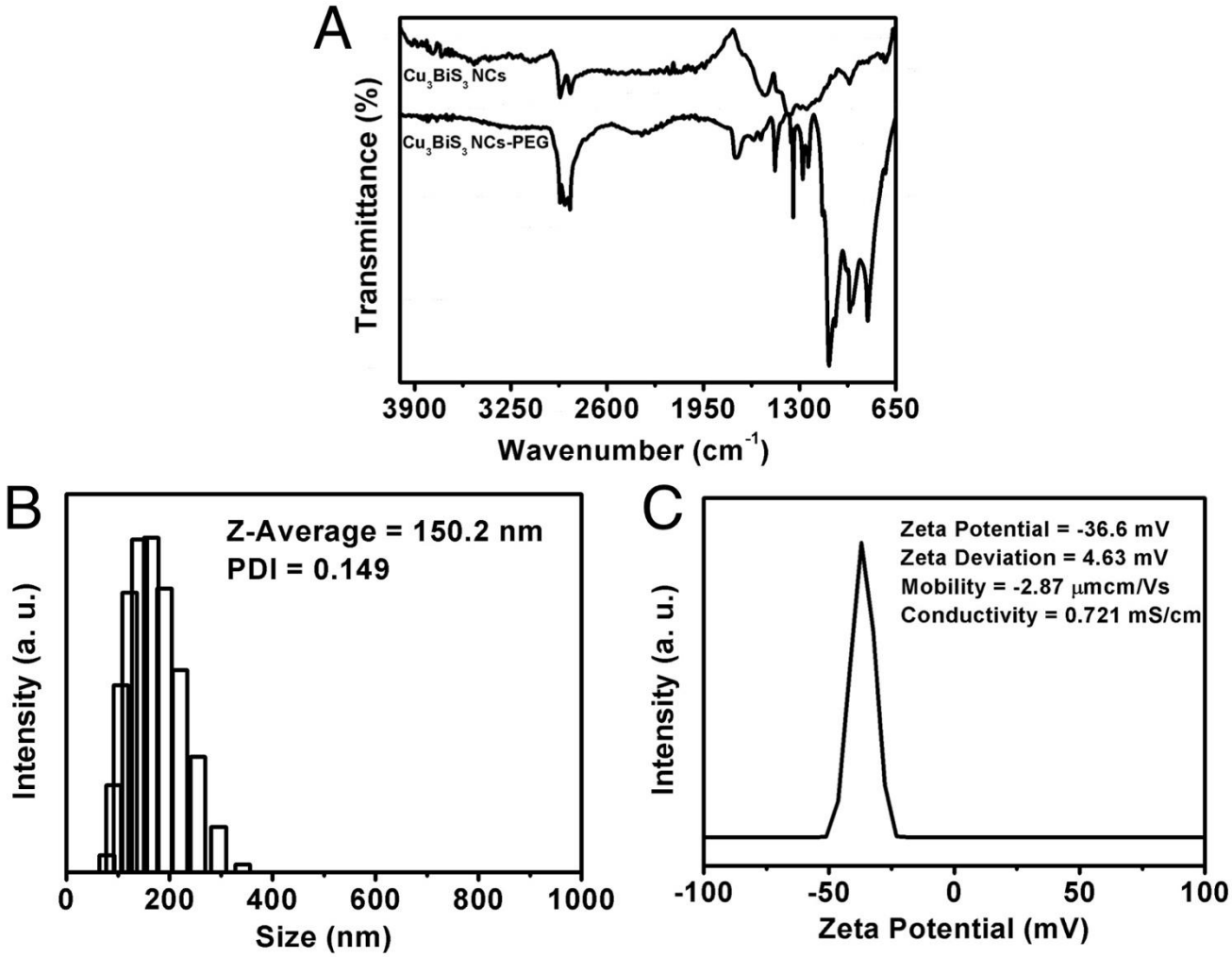

Figure S2. (A) Exhibits the FT-IR spectrum of as-synthesized and PEGylated NCs. **(B)** The hydrodynamic diameter of PEGylated NCs. **(C)** Zeta potential of the PEGylated NCs.

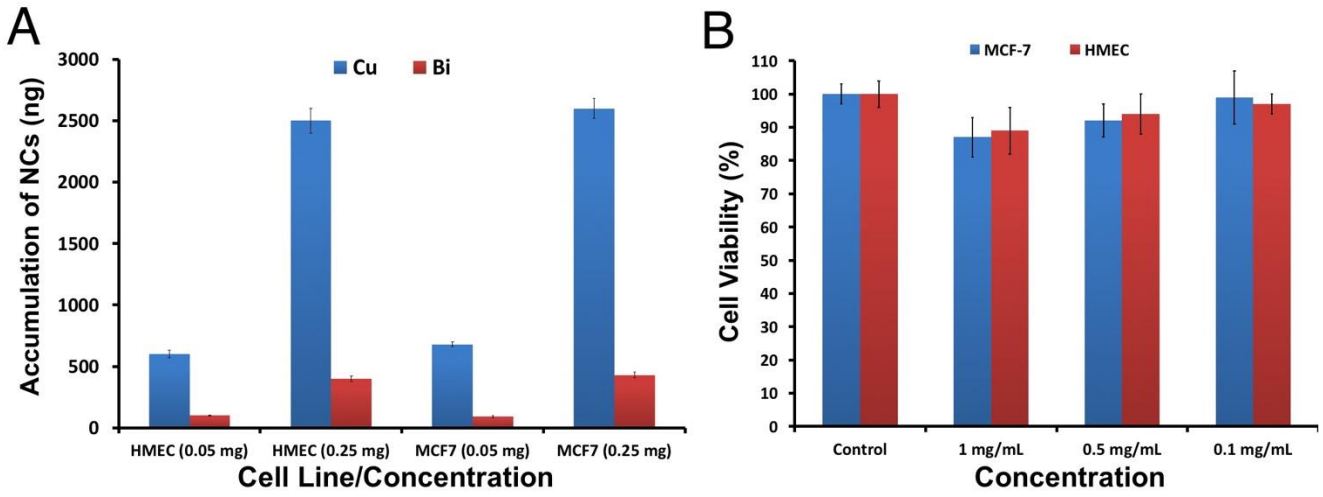

Figure S3. (A) NC uptake by cells was quantified by ICP-MS post 24 h of NC exposure to cells, which was found to be dose-dependent. **(B)** In vitro cell viability analysis of NCs at different concentrations (0.1–1 mg mL^{-1}). The results confirm the cytocompatibility of the PEGylated NCs.

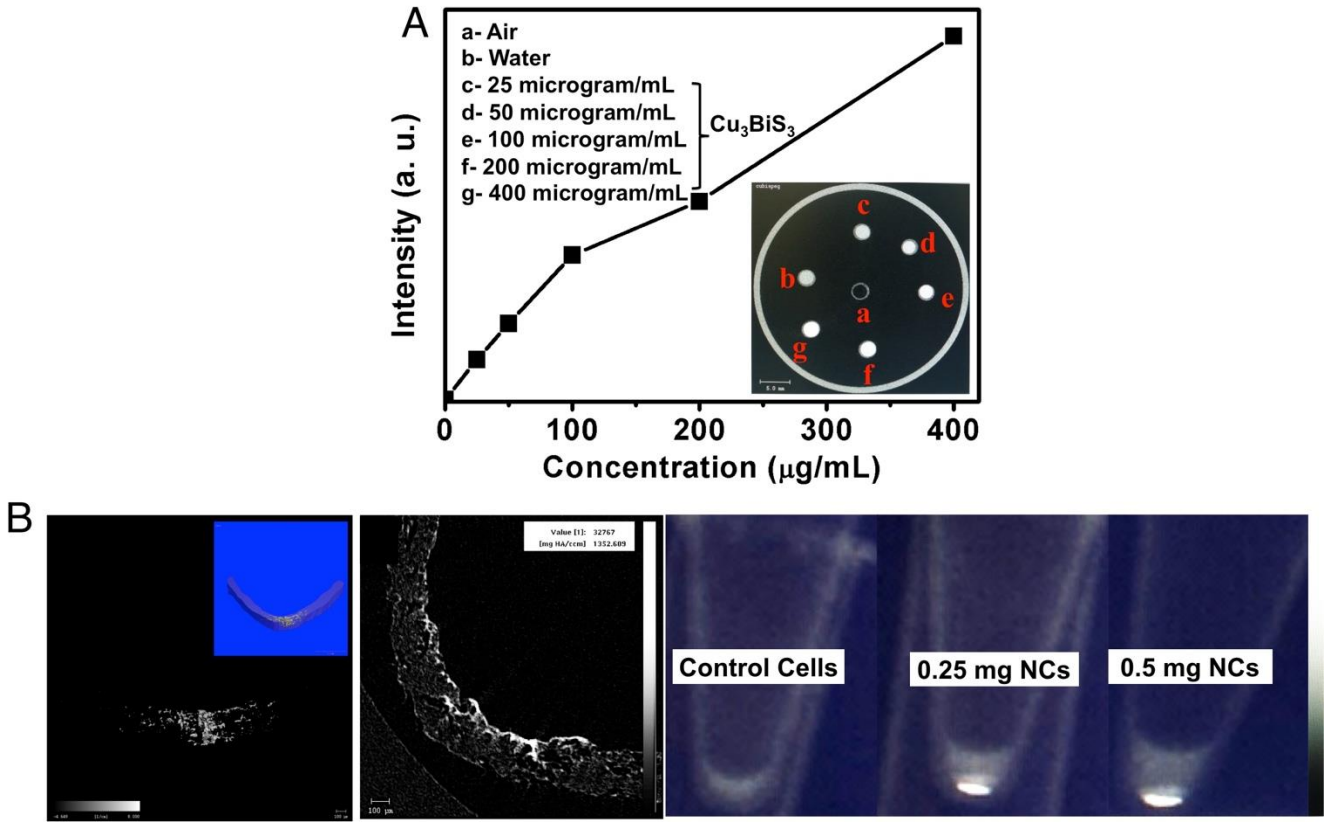

Figure S4. (A) Concentration dependent μCT intensity profile of Cu_3BiS_3 NCs with μCT images of NCs at different concentrations in comparison to air and water (inset). **(B)** μCT slice images of Cu_3BiS_3 NCs loaded on a whatman filter paper-1. The white contrast regions represent the location of the NCs. (inset) 3D reconstruction of the NCs embedded within the paper. The intracellular X-ray μCT imaging performance of NCs was examined with cell pellets that were exposed to NCs, exhibiting discrete and bright contrast when compared to control cells devoid of NCs.

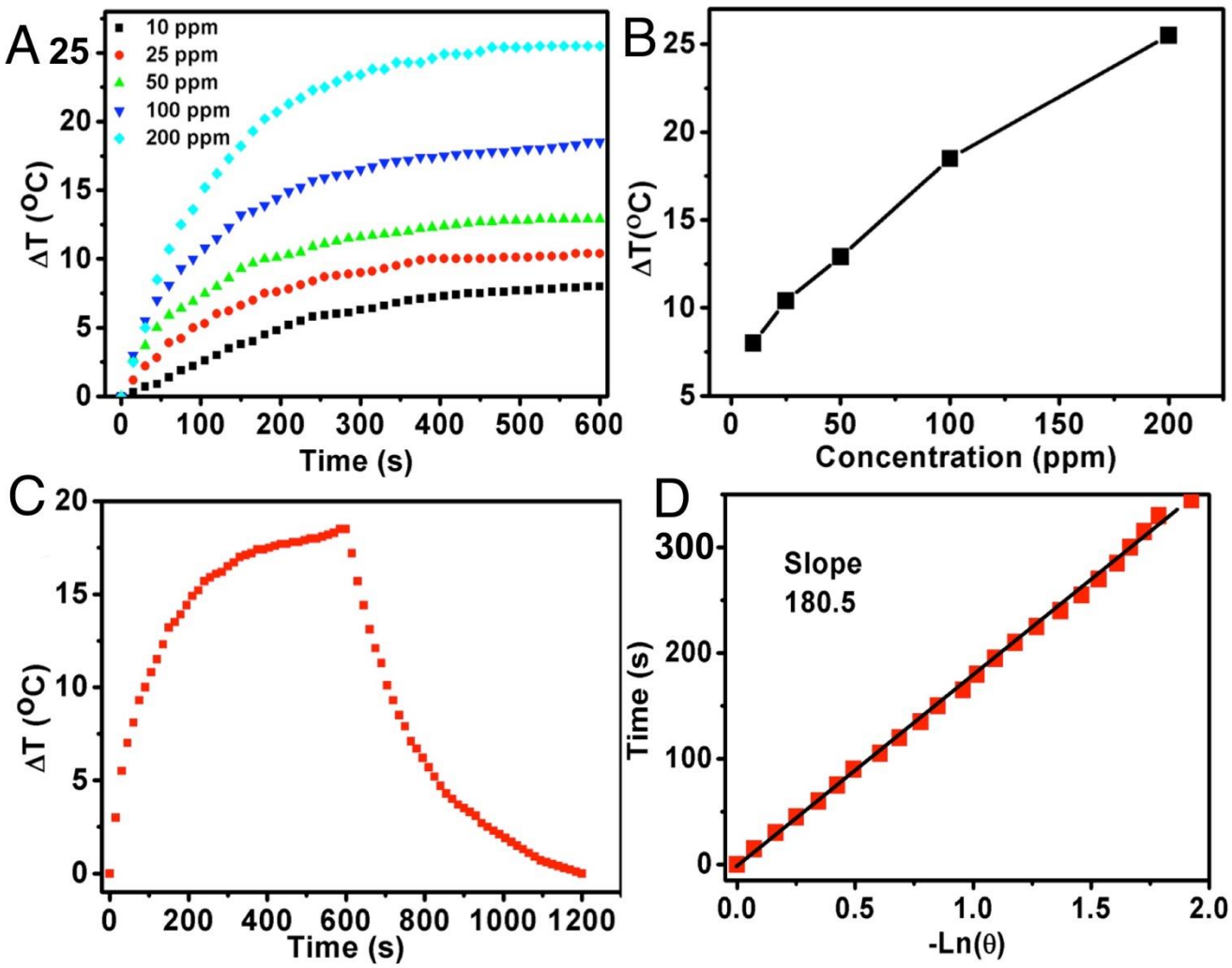

Figure S5. (A) Temperature profiles of NC aqueous solution at different concentrations under NIR irradiation. **(B)** Plot of the temperature change (ΔT) over a period of 600 s versus the concentration of NCs. **(C)** The photothermal response and the cooling curve of the NCs aqueous solution under the irradiation of an NIR laser (800 nm, 1.76 W cm^{-2}) for 600 s and then the laser was shut off. **(D)** Plot of the cooling time versus negative natural logarithm of driving force temperature.

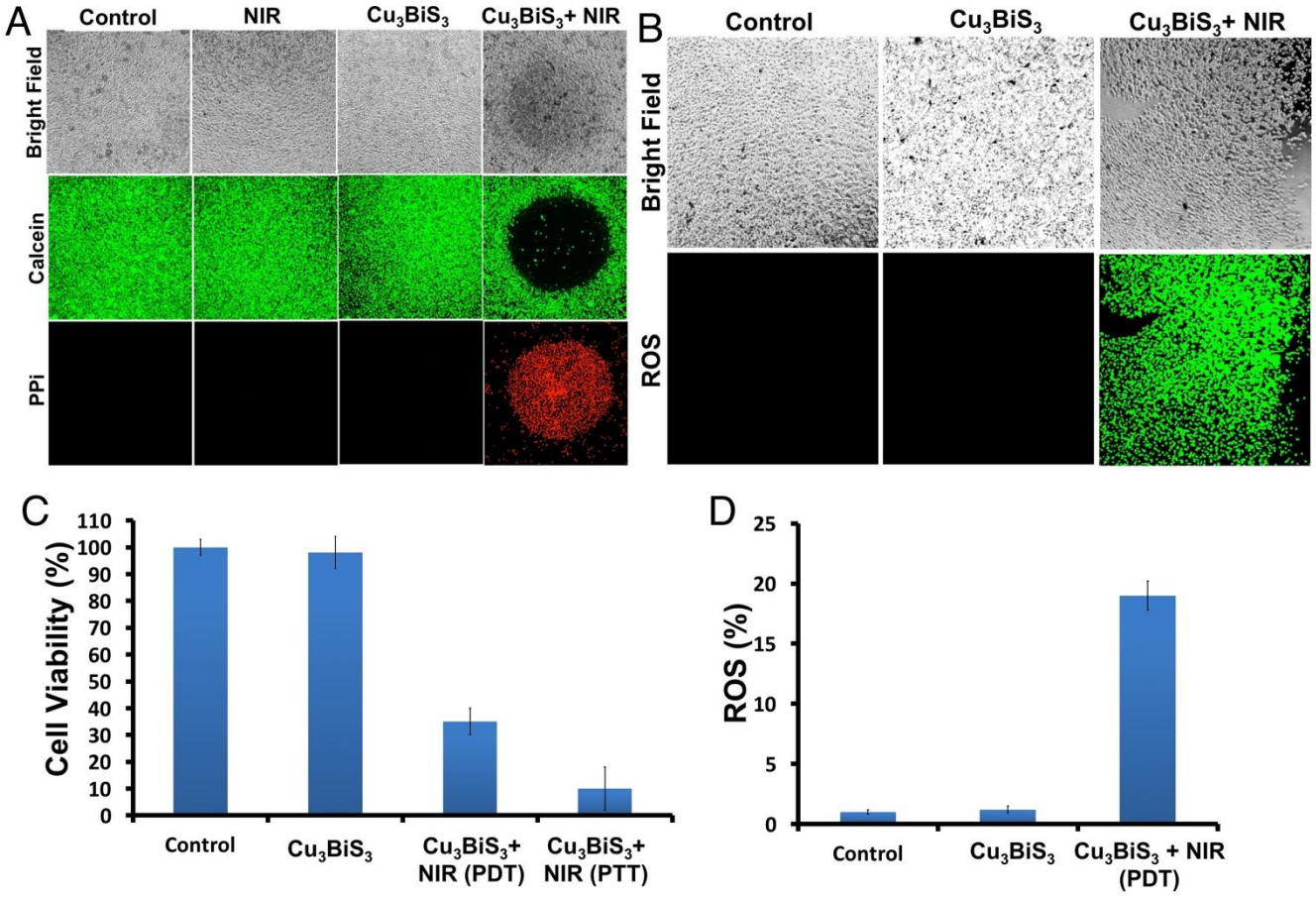

Figure S6. (A) The photothermal competence of NCs was tested on MCF-7 cells with irradiation by an 800 nm NIR laser. The NCs treated cells presented a distinct zone of irradiation, where the laser was incident, demarcating the live cells (calcein stained-green) from the dead (PPi stained-red). The control groups, only laser group and only NC group did not exhibit zone of irradiation as well PPi positive staining. **(B)** ROS generation effect, leading to PDT in vitro. Control and NC group did not exhibit ROS production whereas the NC + NIR group exhibited significant ROS production that can be traced with green-fluorescent ROS tracer, which can also be evidenced by the quantitative data in **(D)**. **(C)** The cell viabilities post NCs exposure, PDT and PTT, clearly depicting the enhanced role of Cu_3BiS_3+NIR (low and high power) in the induction of cell death.

Reference

1. Vankayala R, Lin CC, Kalluru P, Chiang CS, Hwang, KC. Gold nanoshells-mediated bimodal photodynamic and photothermal cancer treatment using ultra-low doses of near infra-red light. Biomaterials. 2014; 35: 5527-38.
2. Wang S, Riedinger A, Li H, Fu C, Liu H, Li L, Liu T, Tan L, Barthel MJ, Pugliese G, Donato FD, Dabbusco MS, Meng X, Manna L, Meng H, Pellegrino T. Plasmonic copper sulfide nanocrystals exhibiting near-infrared photothermal and photodynamic therapeutic effects. ACS Nano. 2015; 9: 1788-800.
3. Kalluru P, Vankayala R, Chiang CS, Hwang KC. Photosensitization of singlet oxygen and in

vivo photodynamic therapeutic effects mediated by pegylated $W_{18}O_{49}$ nanowires. Angew Chem Int Ed. 2013; 52: 12332-6.
4. Guo W, Qiu Z, Guo C, Ding D, Wang TLF, Sun J, Zheng N, Liu S. Multifunctional theranostic agent of $Cu_2(OH)PO_4$ quantum dots for photoacoustic image-guided photothermal/photodynamic combination cancer therapy. ACS Appl Mater Interfaces. 2017; 9: 9348-58.
5. Vijayaraghavan P, Liu CH, Vankayala R, Chiang CS, Hwang KC. Designing multi-branched gold nanoechinus for NIR light activated dual modal photodynamic and photothermal therapy in the second biological window. Adv Mater. 2014; 26: 6689-95.
6. Guo W, Guo C, Zheng N, Sun T, Liu S. Cs_xWO_3 nanorods coated with polyelectrolyte multilayers as a multifunctional nanomaterial for bimodal imaging-guided photothermal/photodynamic cancer treatment. Adv Mater. 2017; 29: 1604157.
7. Li L, Rashidi LH, Yao M, Ma L, Chen L, Zhang J, Zhang Y, Chen W. CuS nanoagents for photodynamic and photothermal therapies: phenomena and possible mechanisms. Photodiagnosis Photodyn Ther. 2017; 19: 5-14.
8. Zhang D, Wen L, Huang R, Wang H, Hu X, Xing, D. Mitochondrial specific photodynamic therapy by rare-earth nanoparticles mediated near-infrared graphene quantum dots. Biomaterials. 2018; 153: 14-26.
9. Zhang M, Cui Z, Song R, Lv B, Tang Z, Meng X, Chen X, Zheng X, Zhang J, Yao Z, Bu W. $SnWO_4$-based nanohybrids with full energy transfer for largely enhanced photodynamic therapy and radiotherapy. Biomaterials. 2018; 155: 135-44.